Detection of sub-ppm Concentrations of Ammonia in an Ionic Liquid: Enhanced Current Density Using 'Filled' Recessed Microarrays

Ghulam Hussain and Debbie S. Silvester*

Nanochemistry Research Institute, Department of Chemistry, Curtin University, GPOBox U1987, Perth, Western Australia 6845

Submitted to Analytical Chemistry

*Author to whom all correspondence should be addressed

E.mail: d.silvester-dean@curtin.edu.au

Tel: +61 (0) 892667148

FAX: +61 (0) 892662300

Abstract

The voltametric detection of less than 1 ppm of ammonia gas in the room temperature ionic liquid (RTIL) 1-ethyl-3-methylimidazolium bis(trifluoromethylsulfonyl)imide ($[C_2mim][NTf_2]$) is demonstrated using low-cost planar electrode devices. Three commercially-available planar devices were employed, all with platinum (Pt) working electrodes: a thin-film electrode (TFE), screen-printed electrode (SPE) and micro-array thin film electrode (MATFE), along with an "ideal" conventional Pt microdisk electrode for comparison. The microholes on the recessed MATFE were also 'filled' with electrodeposited platinum, to improve radial diffusion characteristics to the microhole, and generate higher current densities. Current density was lowest for the TFE and SPE surfaces (linear diffusion), higher for the MATFE (mixed radial and linear diffusion) and even higher for the filled MATFE (predominantly radial diffusion).

Linear sweep voltammetry (LSV) and potential-step chronoamperometry (PSCA) at 10-100 ppm NH_3 gave linear behaviour for current vs concentration. Limits of detection (LODs) were in the range of *ca.* 1-9 ppm, lower than minimum exposure limit (25 ppm) for NH_3. The best stability, reproducibility and the lowest LODs were observed on the recessed and filled MATFEs. These were employed to detect lower concentrations of ammonia (0.1-2 ppm), where linear behaviour was also observed, and LODs of 0.11 (recessed) and 0.02 (filled) were obtained. These are believed to be the lowest LODs (to date) reported for ammonia gas in neat ionic liquids. This is highly encouraging and suggests that RTILs and low-cost miniaturised MATFEs can be combined in amperometric sensor devices to easily and cheaply detect ammonia gas at ppb concentrations.

1. Introduction

The detection of ammonia (NH_3) gas at low concentrations is of great importance due to its high toxicity and use in a wide range of industries e.g. oil and gas, fertilizer, refrigeration etc.[1] Concentrations as low as 500 ppm can be lethal, and the current (USA) Occupational Safety and Health Administration Permissible Exposure Limit (OSHA PEL) for NH_3 is 25 ppm in the gas phase. Although a range of different strategies can been employed to monitor toxic gases,[1,2] electrochemical gas sensors are popular due to their low cost, portability, low power consumption, high sensitivity and selectivity and ability to be miniaturised.[3,4] Commercially available amperometric gas sensors (AGSs) for ammonia are sold by a range of companies,[5] but a major drawback is that the solvent/electrolyte combination (typically water/sulphuric acid) can dry-up (particularly in hot and dry environments) and decrease the sensor lifetime. As a result, non-volatile room temperature ionic liquids (RTILs) have been attracting attention[6-12] as replacement electrolytes in "membrane-free" AGSs. An advantage of using RTILs for gas sensing, is that polar gases such as ammonia are highly soluble,[13] which may be beneficial for detection at very low concentrations.

The reaction mechanism for ammonia oxidation in ionic liquids has been well studied at higher (percent) ammonia concentrations in ionic liquids on Pt microdisk,[14,15] and also on screen-printed electrodes.[16] However, studies focussed on the sensing of ammonia in ionic liquids at low concentrations (less than 100 ppm) electrodes using voltammetry/amperometry techniques are rather limited. Carter et al.[17] employed a home-made prototype printed gas sensor using a constant biasing technique (long-term chronoamperometry) for ammonia sensing at 10-1000 ppm. Linear responses (current vs concentration) were observed best in the lower concentration range up to 200 ppm. A limit of detection (LOD) of 2 ppm was calculated based on the calibration curve in the 10-50 ppm concentration range. The same group[18] reported another printed AGS for detecting ammonia in three different ionic liquids. LODs of 0.12-0.47 ppm were reported from calibration graphs in the 10-40 ppm concentration range, again using a constant biasing technique.

Oudenhoven et al.[19] later reported the sensing of ammonia on a planar interdigitated Pt electrode using a thin layer (5 μm thick) of RTIL. Concentrations down to 1 ppm could be distinguished from the blank response, and it was suggested that cyclic voltammetry was the preferred technique over amperometry, due evidence of electrode fouling for amperometry during exposure to ammonia.

The abovementioned work, in addition to various other studies,[20-23] has shown that there is continuous drive towards the miniaturisation of sensing devices. The ease and low-cost of manufacturing, and their usefulness in applications where portability is essential (e.g. wearable sensors)[24] is driving research in this area. As a result, we are investigating new low-cost, miniaturised, commercially available thin-film electrode surfaces. Their small size means that only a few microliters (or less) of RTIL solvent is needed. Three different types of commercially available planar electrodes have been employed in this work and one of the devices has also been modified with electrodeposited platinum, to enhance the analytical performance. The results from this work will help to determine whether low-cost miniaturised electrodes with RTILs can be used in the design of cheap, portable and robust gas sensors for ammonia, and in particular, which electrode geometry and electrochemical technique is the most favourable.

2. Experimental Section

2.1 Chemical Reagents.

All chemicals were commercially available and used as received. Ethanol (EtOH, 99 %, Sigma Aldrich), acetone (99%, Sigma Aldrich), sulfuric acid (98% w/w [18.4 M], Sigma Aldrich), zinc chloride ($ZnCl_2$, 40 % w/v, Sigma Aldrich, used as a soldering flux for connecting wires with electrodes), chloroplatinic acid hydrate ($H_2PtCl_6.xH_2O$, anhydrous, trace metal basis, ≥ 99.9 %, Sigma Aldrich), ferrocene ($Fe(C_5H_5)_2$, 98 % purity, Fluka) and tetra-*N*-butylammonium perchlorate (TBAP, 98 % purity, Sigma Aldrich) were used as received. The room temperature ionic liquid (RTIL) 1-ethyl-3-methylimidazolium bis(trifluoromethylsulfonyl)imide ($[C_2mim][NTf_2]$, high purity grade), was purchased from Merck, Kilsyth, Victoria, Australia. Ultrapure water with a resistance of 18.2 MΩcm was prepared by an ultrapure water purification system (Millipore Pty Ltd., North Ryde, NSW, Australia). Acetone (>99.9 %, Sigma-Aldrich) was used for washing the electrodes before and after use. Ammonia gas cylinders (2000 ppm and 50 ppm, in nitrogen) were purchased from CAC gases (Auburn, NSW, Australia). Nitrogen gas (for further dilution of NH_3) was obtained from a ≥ 99.99 % high purity compressed nitrogen cylinder (BOC gases, Welshpool, WA, Australia).

2.2 Electrochemical Experiments.

All experiments were performed at laboratory room temperature (294±1 K) in a fume cupboard, inside an aluminium Faraday cage to reduce electrical interference. A PGSTAT101 Autolab potentiostat (Eco, Chemie, Netherlands) interfaced to a PC with Nova 1.11.2 software was employed. Platinum (Pt) thin-film electrodes (TFEs) and Pt microarray thin-film electrodes (MATFEs) were obtained from Micrux Technologies, Oviedo, Spain (ED-SE1-Pt and ED-mSE-10-Pt, respectively*)*. The TFE and MATFE from Micrux have the same design (1mm diameter Pt working electrode, Pt reference and Pt counter electrodes), except the working electrode of the MATFE is covered with a layer of SU-8 resin into which 90 µ-holes of 10 µm diameter are drilled to create 90 recessed microelectrodes. The centre-to-centre spacing of the µ-holes is 100 (±1) µm

(10× the diameter). In both the TFE and MATFE, the Pt thin-film (150 nm thickness) was fabricated by thin-film technology on a Pyrex substrate. Pt screen-printed electrodes (SPEs) were obtained from DropSens, Spain (DRP-550), and consisted of a Pt-based WE (4 mm diameter), a Pt CE and a Ag quasi-RE. The screen-printed paste consists of conductive Pt particles, binding materials and solvents, but the manufacturer does not disclose the exact chemical composition.

The TFEs and MATFEs were electrochemically activated in 0.5 M $H_2SO_{4\,(aq)}$ by scanning the potential between -0.21 and +1.3 V (TFE), or -0.27 and + 1.4 V (MATFE) vs an external Ag/AgCl (0.1 M KCl) reference electrode (BASi, Indiana, USA) and Pt coil counter electrode (Cambridge Ltd., UK) at a sweep rate of 50 mVs^{-1} for ca. 200 cycles. The electrodes were washed with ultrapure water and dried under a stream of nitrogen. The Pt SPE was used "as is" (without electrochemical activation or pre-treatment), as recommended by the manufacturer. The microholes of the MATFE were filled with Pt by depositing from a 5 mM solution of H_2PtCl_6 in 0.5 M H_2SO_4, starting from the open circuit potential, then holding the potential at -0.05 V (vs an external Ag/AgCl reference electrode and Pt wire counter electrode) for 300 seconds, under fast magnetic stirring to ensure a constant rate of flux. For gas sensing experiments, the planar electrodes were placed into a modified rubber bung and inserted into the glass cell (a modified version of a T-cell).[25] 2 µL of RTIL was drop-cast on the TFE and MATFE, and 8 µL on the SPE. Prior to the introduction of ammonia, the cell was purged with nitrogen to remove dissolved gases and impurities. When the baseline was stable (after ca. 20 minutes), ammonia gas was introduced into the cell and continuously flowed over the electrode.

For experiments on the microdisk electrode, a conventional home-made Pt microelectrode (16.6 µm diameter) was employed. The electrode was polished on soft polishing pads (Buehler Illinois) with decreasing size of alumina powder (3 µm, 1 µm and 0.5 µm, Kemet, NSW, Australia). The diameter was calibrated electrochemically using 1mM ferrocene (deaerated) in acetonitrile with 0.1 M TBAP vs a silver wire reference electrode and a Pt coil counter electrode. A disposable micropipette tip was fixed at the top of Pt microelectrode to provide a cavity into which 25 µL of

$[C_2mim][NTf_2]$ was placed. The electrode was housed in a specially designed glass T-cell[26,27] with a Ag wire (combined counter and quasi-reference electrode) inserted in from the top. The cell was purged under vacuum (Edwards high vacuum pump, Model ES 50) for ca. 90 minutes to remove dissolved impurities (e.g. oxygen or water) present in the ionic liquid. When a clean blank voltammogram was obtained, ammonia gas was introduced into the cell.

2.3 Gas Mixing System.

In order to obtain different concentrations of ammonia, cylinders of ammonia standards (2000 ppm and 50 ppm, nitrogen fill), were diluted with nitrogen using a gas mixing system as reported previously by our group.[16,25] This consists of two digital flow meters one for ammonia (0-1.0 L/min, John Morris Scientific, NSW, Australia), and one for nitrogen (0-10 L/min, Aalborg, New York USA), with a gas-mixing segment to increase turbulence and ensure adequate mixing of the gases. The relative flow rates were used to calculate the different concentrations of ammonia introduced into the T-cell. A sufficiently long time (ca. 25 minutes initially, and 10 mins between concentration changes) was left in order to ensure complete saturation of the gas in the ionic liquid and obtain a stable current. It is noted that the time for saturation may be less than this, but measuring response times will be the focus of future publications.

2.4 Electrode Imaging

Scanning electron microscopy (SEM) experiments were performed on the working electrodes of the three planar devices (TFE, SPE and MATFE), and on the filled MATFE. SEM Images were obtained using Zeiss Evo 40XVP model, with a voltage of 2.0 kV (see Figure 1). Atomic force microscopy (AFM) was performed using a Bruker FastScan instrument on the MATFE to image the geometry and depth of the µ-holes, and the filling of the µ-holes, and analysed using NanoScope analysis 1.5 software. The resolution of the instrument is up to 10 µm in height (Z-range, Icon AFM Scanner).

3. Results and Discussion

3.1 Characterisation of electrode surfaces using SEM and AFM

In this study, three types of commercially available planar electrode devices (all with Pt working electrodes) have been employed - thin-film electrode (TFE), screen-printed electrode (SPE) and microarray thin-film electrode (MATFE), along with a modified MATFE (where Pt has been electrodeposited into the microholes to create almost inlaid electrodes), and a conventional microdisk electrode. Figure 1 shows scanning electron microscopy (SEM) images for the different electrode surfaces employed. It was not possible to obtain an image for the microdisk electrode due to its large size and inability to fit into the SEM machine. The image on the TFE (Figure 1a) shows a very flat and smooth surface, which is highly beneficial for reproducible electrochemical experiments, and shows the high quality of the manufacturing process. Atomic Force Microscopy (AFM) of these surfaces revealed some very small features on the surface, with heights of ca. 10 nm, and may be small defects from the Pt sputtering process or during packaging and transportation. In contrast, the SPE surface (Figure 1b) is very rough and porous, due to the electrode material being made of a mixture ("paste") of conductive Pt particles, polymeric binding materials and solvents, as reported previously.[25,28] The height of the paste was out of the range of the AFM machine, indicating that it is > 10 μm thick. The MATFE (Figure 1c) has the same underlying Pt surface as the TFE, but it is covered with a layer of SU-8 polymer, into which 90 microholes of 10 μm in diameter are created, leaving 90 recessed electrodes; Figure 1c shows a section of the whole array. Depth profiling with AFM revealed that the thickness of the SU-8 layer was consistent across each device, but varied between 2.6 and 3.4 μm on different electrodes (sample size of 5), which is within the manufacturer's statement of 3±0.5 μm. Figure 1d (top) shows a close-up image of one microhole of the MATFE, and Figure 1d (bottom) shows an image of one microhole that has been filled with electrodeposited Pt to create an almost inlaid electrode array. It is expected that the filled arrays will provide enhanced radial diffusion characteristics of analyte species towards the electrode, and will give improved analytical responses compared to the recessed

MATFE. Details of the deposition process are shown in the experimental section and a small discussion is given below.

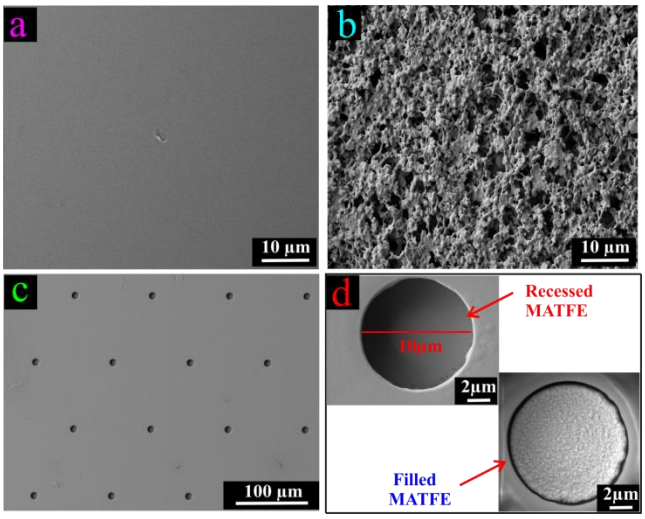

Figure 1. Scanning electron microscopy (SEM) images of a Pt (a) TFE, (b) SPE and (c) MATFE. The MATFE consists of a Pt TFE covered by an inert layer of SU-8 polymer with holes to create 90 recessed Pt microdiscs (depth = 3±0.5 µm, diameter = 10 µm). Figure (d) shows close-up SEM images of a recessed microhole, and a filled microhole (holes were filled by electrodeposition from a solution of 5 mM H_2PtCl_6 in 0.5 M H_2SO_4).

Deposition of Pt into the microholes: In order to fill the microholes of the MATFE, the electrode was placed into a solution of 5 mM chloroplatanic acid (H_2PtCl_6) in 0.5 M H_2SO_4, and various deposition parameters were explored. Both pulse and constant potential deposition techniques were carried out, in line with literature reports for Pt nanoparticle deposition.[29-32] Constant potential deposition was chosen since it gave the most stable and reproducible deposits (noting that the size of the deposits were on the micrometer (not nanometer) scale, due to the size of the microholes). It was found that if the overpotential was too high, or the deposition time was too long, cauliflower-shaped deposits were obtained. During this process, the holes were observed to fill preferentially around (and then over) the edges of the pores, with very little deposit in the centre of the pore. The final deposition parameters (given in the experimental section) involved holding at the open circuit potential (OCP = 0.75 V), followed by deposition in the kinetically controlled region (-0.05 V vs Ag/AgCl) holding for 5 minutes, under fast magnetic stirring to keep the rate of flux uniform and to produce controlled (slow) growth of the nucleation sites. AFM revealed that the hole was uniformly filled from the centre to the edges, up to a depth of ca. 0.9 µm below the surface (noting that the

diameter of the pores is 10 μm). This amount of filling was enough to produce the desired radial diffusion characteristics (see below), but without the significant charging/capacitative currents that were observed with the cauliflower shaped deposits.

3.2 Electrochemical Oxidation Mechanism for Ammonia on the Planar Electrode Devices.

The RTIL [C_2mim][NTf_2] was chosen as the solvent/electrolyte in this work due to its wide electrochemical window (> 4.5 V), good chemical and thermal stability, high intrinsic conductivity and lowest viscosity of the RTILs available in our laboratory. The electrochemical response for ammonia oxidation in this RTIL (at higher concentrations) has also been well studied.[14-16] Before undertaking analytical studies on the new planar electrode devices employed in this work, the electrochemical reaction mechanism for ammonia should first be understood. It is noted here that there was a different mechanism for oxygen reduction in [C_2mim][NTf_2] on DropSens Pt screen-printed electrodes (compared to conventional Pt macrodisk electrodes).[25] This was suggested to be a reaction of the electrogenerated superoxide with the imidazolium cation, catalysed by compounds present in the paste of the SPE. However, no unusual reaction was observed to take place for oxygen on Pt TFEs[33] and MATFEs.[20] For ammonia, the mechanism on SPEs was found to be the same as on conventional Pt electrodes in our previous work,[16] but the behaviour on TFEs and MATFEs has not yet been reported.

Figure 2 shows cyclic voltammograms (CVs) at 100 mVs^{-1} for the oxidation of 500 ppm ammonia on the five Pt electrodes employed in this study: (a) TFE, (b) SPE, (c) μ-disk electrode, (d) recessed MATFE and (e) filled MATFE. In all figures, the dashed red line is the blank CV in the absence of ammonia. According to the number of peaks present in the CVs in Figure 2, the mechanism for ammonia oxidation on all surfaces appears to be the same as that reported previously.[14,15] Firstly, there is a single broad oxidation peak/process between 0.9 to 2.0 V labelled as peak I, followed by two reduction processes, peak II (ca. 0.0 to -0.5 V) and peak III (ca. -0.5 V to -1.0 V), followed by an oxidation peak IV (ca. -0.5 to 0.0 V). It is noted that the variation in

ammonia oxidation peak potential is likely to be due to the different (integrated) quasi-reference electrodes employed. The identities of the peaks are described by the following equations:[14,15]

Peak (I) $$NH_3(g) + 3A^- \rightarrow \frac{1}{2}N_2(g) + 3HA + 3e^- \quad (1)$$

where A^- = the RTIL anion ($[NTf_2]^-$). There is thought to be an equilibrium reaction between the solvated proton (HA) and another ammonia molecule in solution:

$$HA + NH_3(g) \rightleftharpoons NH_4^+ + A^- \quad (2)$$

Two reduction processes can then occur: the reduction of HA (equation 3) or the reduction of NH_4^+ (equation 4).

Peak (II) $$HA + e^- \rightarrow A^- + H(ads) \quad (3)$$

Peak (III) $$NH_4^+ + e^- \rightarrow NH_3(g) + H(ads) \quad (4)$$

Peak IV on the reverse oxidative sweep is believed to be the oxidation of the electrogenerated adsorbed proton.[14,15]

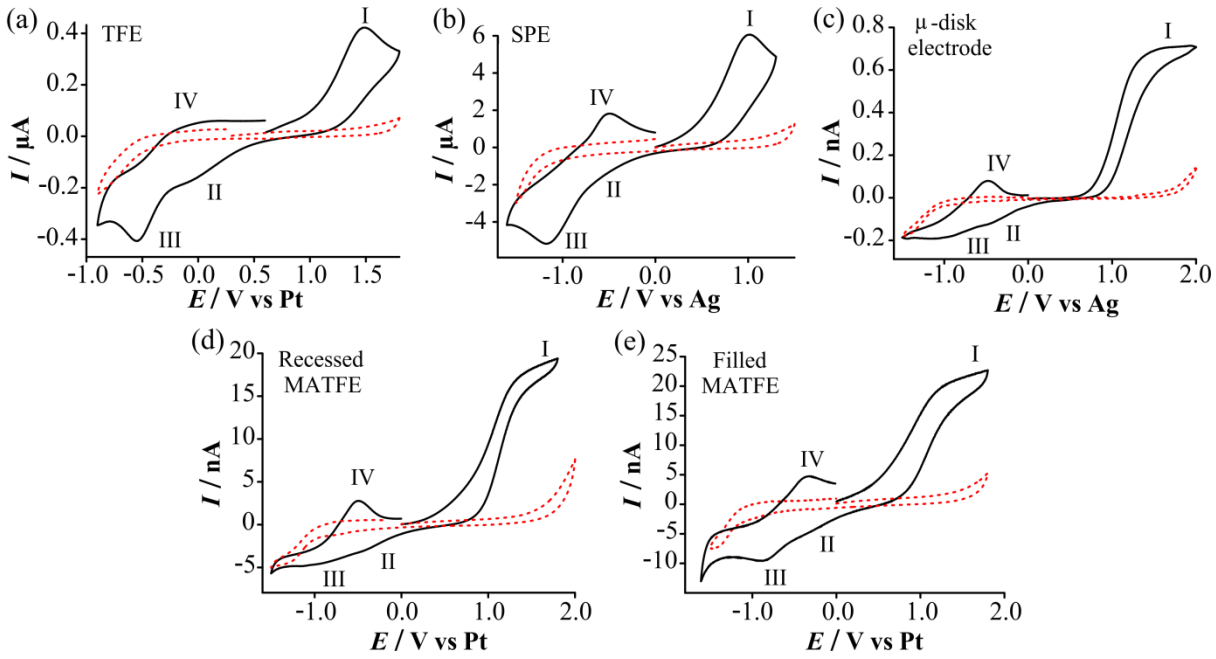

Figure 2. Cyclic voltammetry for 500 ppm ammonia oxidation in $[C_2mim][NTf_2]$ on a Pt (a) TFE (diameter 1mm), (b) SPE (diameter 4 mm), (c) µ-disk electrode (diameter 16.6 µm), (d) MATFE (90 recessed electrodes, diameter 10 µm), (e) MATFE with the recessions filled with electrodeposited Pt. Dashed red line is the response in the absence of ammonia. Scan rate 100 mVs^{-1}.

The shape of all the voltammograms in Figure 2 is similar to that reported previously at higher concentrations of ammonia on microdisk and screen-printed electrodes.[14-16] Peak-shaped oxidation waves were observed on the macro-sized TFE and SPE electrodes, consistent with predominantly linear diffusion occurring at these surfaces. In contrast, a steady-state oxidation wave was obtained on the micron-sized electrodes (recessed and filled MATFEs and Pt µ-disk electrode) due to the increased contribution from radial diffusion. While the response reaches an ideal steady-state plateau on the µ-disk electrode, the response on the recessed MATFE shows a steady-state current response that continues to rise after the plateau. The behaviour of the filled MATFE is somewhere in between, indicating that the holes are almost filled to create inlaid electrodes, but there may be some non-uniformity to the platinum deposit (e.g. holes/pores). A slanted plateau is also observed on nanoarray electrodes in liquid/liquid electrochemistry experiments,[34,35] and although the exact reason is unclear, it could be due to the nature of the electrode array (as opposed to a single electrode), and overlapping diffusion profiles. However, we note that this behaviour was not observed for a more "ideal" redox couple (1mM ferrocene in acetonitrile with 0.1 M TBAP, results not shown) on the MATFE, where true steady-state behaviour was obtained.

3.3 Current Density Comparison

In order to compare the oxidation of ammonia at Pt electrodes of varying size, the current density (*J*) was calculated from the oxidation peak current divided by the electrode area. Figure 3 shows a plot of *J* for 500 ppm ammonia on the five different electrodes. *J* is the smallest for the larger electrodes (1 mm diameter TFE and 4 mm diameter SPE) due to the predominantly linear diffusion occurring at these surfaces. *J* for the µ-disk electrode is significantly higher, as expected due to the faster rate of mass transport (radial diffusion) to micron-sized electrodes.[36] However, *J* for the recessed MATFE is lower than the µ-disk electrode, even though the diameter of each recessed electrode is smaller than the µ-disk electrode diameter. One explanation for this could be the contribution from linear diffusion within the pores, which lowers the current response, as expected for recessed electrodes.[37,38] However, even when the pores are filled to create almost inlaid

electrodes (filled MATFE in Figure 3), *J* is still not as high as expected. This points to the possibility that the geometry of the array is not fully optimised, giving rise to the overlapping of diffusion layers and reducing the expected current. This is consistent with our observations for oxygen reduction on the same MATFE devices.[20] Based on the plot in Figure 2, it is expected that the micron-sized electrodes will provide a better resolution of peak currents at very low concentrations of analyte, so therefore the analytical response of these electrodes was further studied.

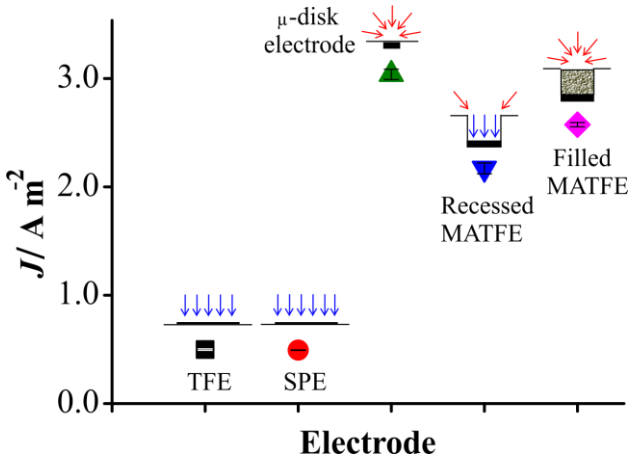

Figure 3. Current density (*J*) plot for the oxidation of 500 ppm ammonia in [C_2mim][NTf_2] on a Pt: TFE (■), SPE (●), μ-disk electrode (▲), recessed MATFE (▼) and filled MATFE (◆). Sketches of the expected diffusion processes (linear, radial and linear and radial combined) based on the electrode geometry are also shown. Error bars are small, and represent 1 standard deviation (n=4).

3.4 Analytical Response for Ammonia on the Planar Electrode Devices

To study the ability for these electrodes to detect ammonia, the analytical utility and sensitivity for ammonia in [C_2mim][NTf_2] was investigated. Two electrochemical techniques (linear sweep voltammetry (LSV) and potential-step chronoamperometry (PSCA)) were carried out on the five different Pt surfaces, to identify what technique and which electrode is the most sensitive towards low (ppm) concentrations of ammonia gas.

3.4.1 Linear Sweep Voltammetry.

Figure 4 shows linear sweep voltammetry (LSV) for the oxidation of 10-100 ppm of ammonia in [C_2mim][NTf_2] on a Pt (a) TFE, (b) SPE, (c) μ-disk electrode (d) recessed MATFE and (e) filled MATFE at a scan rate of 100 mVs^{-1}. The response in the absence of ammonia is shown as a dashed

red line. The insets show the corresponding calibration plots of oxidation current (baseline corrected) vs gas-phase concentration of ammonia. In this lower concentration range, peak-shaped behaviour was still observed on the larger TFE and SPE devices. Steady-state behaviour was observed on the µ-disk electrode (Figure 4c), a slanted steady-state response on the recessed MATFE (Figure 4d), and a more ideal steady-state response on the filled MATFE (Figure 4e). On all of the electrodes, the response at 10 ppm ammonia was clearly distinct from the blank response, which is highly encouraging from an analytical perspective. The calibration graphs showed excellent linearity ($R^2 > 0.998$), with a slightly more curved response on the SPE.

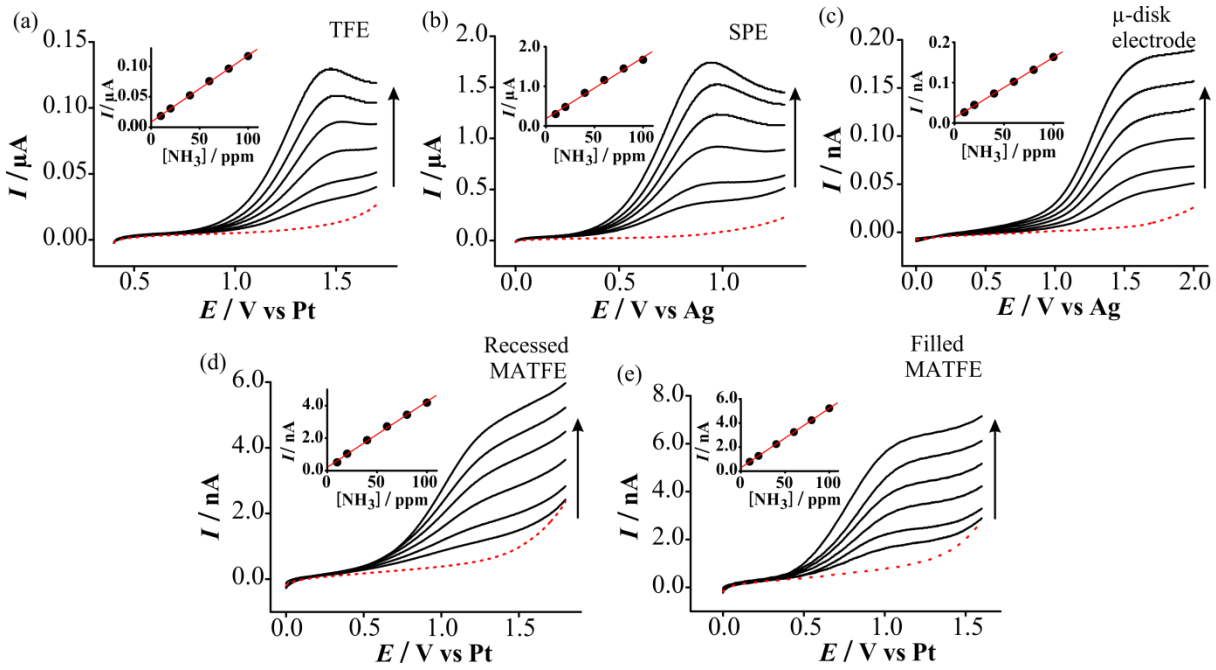

Figure 4. Linear sweep voltammetry (LSV) for the oxidation of ammonia (10-100 ppm) in $[C_2mim][NTf_2]$ on a Pt (a) TFE, (b) SPE, (c) µ-disk electrode (diameter 16.6 µm), (d) recessed MATFE (90 electrodes, diameter 10 µm, depth 3±0.5 µm), (e) MATFE with the recessions filled with electrodeposited Pt at a scan rate of 100 mVs^{-1}. Dotted line is the response in the absence of ammonia. Currents on the recessed MATFE were measured from a fixed potential of 1.4 V, due to the absence of a limiting current plateau. The insets show calibration plots of peak current (baseline corrected) vs concentration, along with the line of best fit.

Table 1 shows the analytical parameters resulting from the calibration graphs in Figure 4. The data was highly reproducible on several days (n=4) with error bars (1 standard deviation) that were <4 % on all surfaces. Sensitivities were calculated from the gradient of the line of best fit and limits of detection (LODs) were calculated using three times standard deviation of the line. The sensitivities were higher on the larger surfaces, as expected. Importantly, the sensitivity of the filled MATFE was > 20 % greater than for the recessed MATFE, indicating that filling the holes is beneficial from

an analytical perspective. The LODs on all surfaces (0.3 to 9.2 ppm) were well below the OSHA PEL for ammonia (25 ppm), and this could further be lowered by studying a lower concentration range, as discussed later. The most important observation from Table 1 is that the recessed and filled MATFEs give the lowest LODs, and therefore these electrodes have been chosen to detect ammonia at even lower concentrations (see section 3.5).

Table 1. Analytical parameters (sensitivity and limit of detection, LOD) calculated for ammonia oxidation (10-100 ppm) on different Pt electrodes using linear sweep voltammetry (LSV) and potential-step chronoamperometry (PSCA). Data obtained from the 0.1-2 ppm range is also included for the MATFEs.

Electrode	LSV		PSCA	
	Sensitivity / $Appm^{-1}$	LOD / ppm	Sensitivity / $Appm^{-1}$	LOD / ppm
TFE	1.1×10^{-9}	2.7	5.6×10^{-10}	2.5
SPE	1.6×10^{-8}	9.2	7.4×10^{-9}	4.5
μ-disk electrode	1.5×10^{-12}	2.7	1.8×10^{-12}	2.5
Recessed MATFE	4.0×10^{-11}	2.0 (0.11)*	4.0×10^{-11}	2.1
Filled MATFE	4.9×10^{-11}	0.3 (0.02)*	4.1×10^{-11}	1.5

* calculated from the calibration graph at the 0.1-2 ppm range

3.4.2 Potential-Step Chronoamperometry.

Under the same experimental conditions as for LSV, potential-step chronoamperometry (PSCA) was also carried out. Figure 6 shows PSCA transients for 10-100 ppm ammonia oxidation in $[C_2mim][NTf_2]$ on a Pt (a) TFE, (b) SPE, (c) μ-disk electrode, (d) recessed MATFE and (e) filled MATFE. The red dotted line is the response in the absence of ammonia. The potential was stepped from 0 V to an appropriate value after the peak (or on the current plateau), and measured for 10 seconds. For simplicity, the current response was measured as an average of the last 100 milliseconds of the transient. The corresponding calibration graphs (baseline corrected current vs concentration) are shown in the insets of the figures, and excellent linearity was observed, with $R^2 > 0.999$.

The transients for the larger TFE and SPE surfaces (Figure 6a and 6b) show typical Cottrellian behaviour,[36] where I is $\propto D^{1/2}$. In comparison, the current transients for the Pt μ-disk electrode (Figure 6c) have two different time regimes, where I is $\propto D^{1/2}$ at short times and I is $\propto D$

at longer times, described by the Shoup and Szabo expression.[39] We note that the experimental data on the µ-disk electrode was attempted to be fitted to the Shoup and Szabo expression, [39] but was unsuccessful due to the complicated mechanism, consistent with a previous report.[15] The shape of the transients on the recessed MATFE (figure 5d) are similar to that on the µ-disk electrode, but there is a much more abrupt change in current between the two time regimes. This behaviour has been reported to be due to the recessed nature of the working electrode.[35,38] The transient on the filled MATFE is somewhere in between the µ-disk electrode and the recessed MATFE, consistent with the shapes of the LSV in Figure 4.

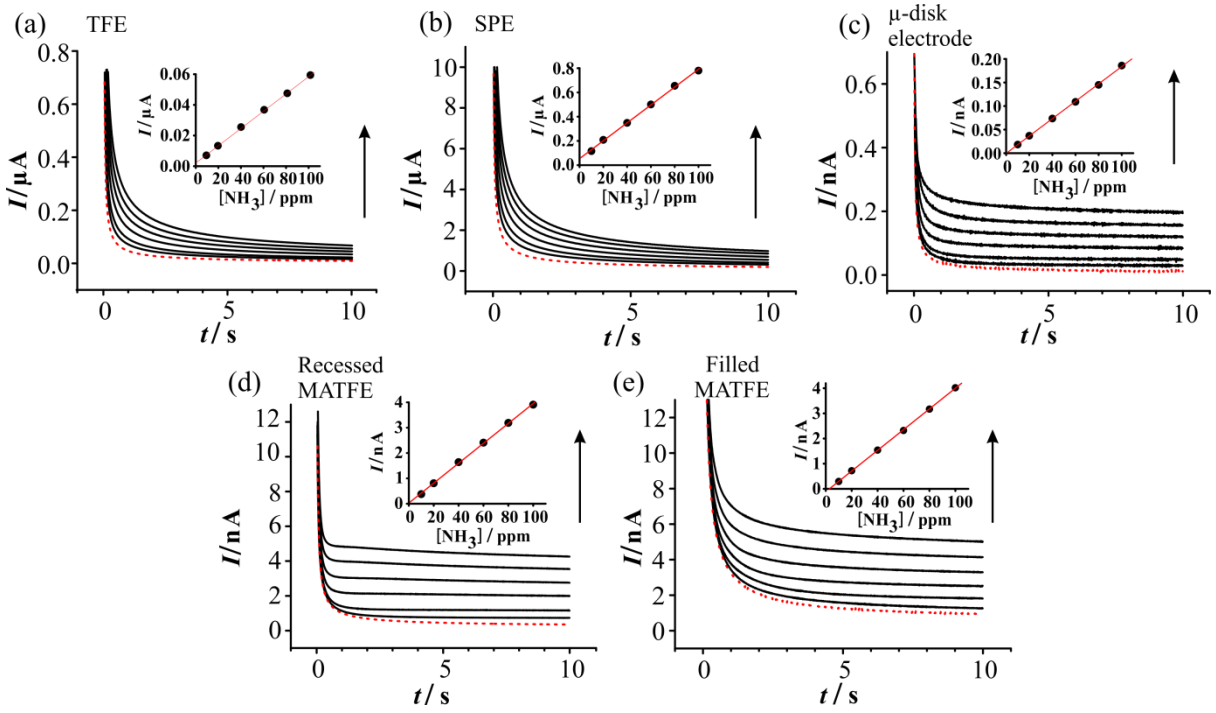

Figure 5. Potential-step chronoamperometry (PSCA) for the oxidation of ammonia (10-100 ppm) in [C_2mim][NTf_2] on a Pt (a) TFE, (b) SPE, (c) µ-disk electrode, (d) recessed MATFE and (e) filled MATFE. The potential was stepped from 0 to (a) + 1.6 V, (b) + 1.1 V, (c) + 1.9 V, (d) + 1.5 V and (e) 1.4 V. Dotted line is the response in the absence of ammonia. The insets are the corresponding calibration plots of current (averaged over the last 10 data points) vs concentration, along with the line of best fit.

The analytical parameters obtained from the PSCA experiments are shown in Table 1. The sensitivities were highest on the larger electrodes, and lowest on the (single) µ-disk electrode. There was some improvement in the LODs using PSCA compared to LSV, except on the MATFEs, where LSV was slightly superior. For PSCA, the LODs on all surfaces (1.5 to 4.5 ppm) were significantly lower than the permissible exposure limit of 25 ppm for ammonia.

3.5 Low concentration study on recessed and filled MATFEs using LSV

Since LSV on the recessed and filled MATFEs gave the lowest LODs, this technique and these electrodes were used for further studies at lower concentrations to examine the true limit of detection. Figure 6 shows linear sweep voltammetry for the oxidation of ammonia from 0.1 to 2 ppm, with the response in the absence of ammonia shown as the red dotted line. Plots of current vs concentration are shown as insets to the figure. Even at concentrations of less than 1 ppm, the response for ammonia oxidation is clearly distinct from the blank response. In contrast, on the larger electrodes (TFE and SPE), current responses at this concentration were much more difficult to observe above the noise. Additionally, the current on the (single) microdisk electrode was extremely small and too low to measure accurately with the standard potentiostat.

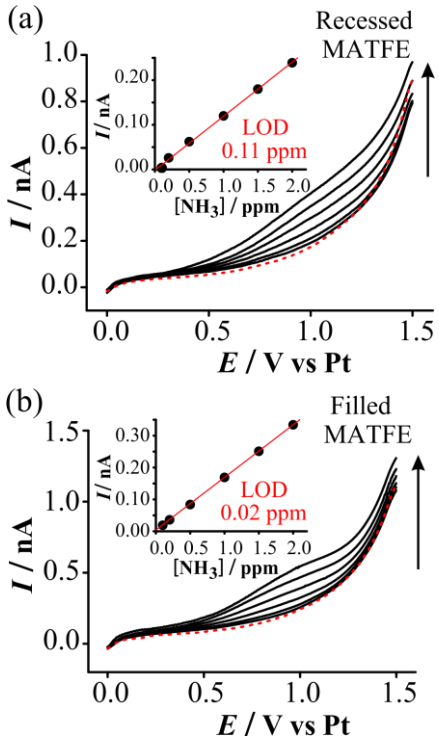

Figure 6. LSV for the oxidation of ammonia in $[C_2mim][NTf_2]$ at low concentrations (0.1 to 2 ppm) on a Pt (a) recessed MATFE and (b) filled MATFE. The red dotted line is the response in the absence of ammonia. The insets show calibration plots of peak current (baseline corrected) vs concentration, along with the line of best fit.

The shape of the voltammetry is clearly more steady-state like on the filled MATFE (Figure 6b) compared to the recessed MATFE (Figure 6a) at these low concentrations, and the current is also larger (higher sensitivity), supporting the suggestion of the larger contribution from radial

diffusion on the filled MATFE. This increased sensitivity has resulted in an improvement in the LOD for ammonia from 0.11 ppm (recessed MATFE) to 0.02 ppm (filled MATFE). This is a very significant result, since these LODs are one order of magnitude lower than that reported previously for ammonia in ionic liquids,[17-19] and opens up the possibility to use these cheap planar electrode devices for trace detection of ammonia gas at concentrations much less than 1 ppm. It is noted that ppb detection limits have been reported previously for ammonia using a low-cost chemoresistive sensor based on single-walled carbon nanotubes,[40] but this is believed to be the first time that ammonia has been detected at such low concentrations using an amperometric technique.

Conclusions

The electrochemical oxidation ammonia has been studied in $[C_2mim][NTf_2]$ on four different types of Pt planar electrode devices (three commercially-available and one modified surface), with the reaction mechanism appearing to be the same as on conventional μ-disk electrodes. Current density was the smallest on the large TFE and SPE surfaces, but much higher on the μ-disk and MATFE surfaces. Calibration graphs obtained from 10-100 ppm ammonia were linear on all surfaces, with the lowest LODs found on the filled and recessed MATFEs using linear sweep voltammetry. These electrodes were subsequently used to investigate even lower concentrations from 0.1 to 2 ppm, giving the lowest limits of detection for ammonia in ionic liquids to date (20 ppb on the filled MATFE). Not only were all of the electrodes able to easily detect concentrations lower than the permissible exposure limit (25 ppm), but the filled MATFE was capable of detecting sub ppm concentrations, opening up the possibility of using ionic liquids and planar electrode devices for accurate monitoring of ammonia at trace concentrations.

Author Information

Corresponding Author - E-mail: d.silvester-dean@curtin.edu.au

Acknowledgments

GH thanks Curtin University, the Department of Chemistry and the Nanochemistry Research Institute (NRI) for a PhD scholarship. DSS thanks the Australian Research Council (ARC) for a

Discovery Early Career Researcher Award (DECRA: DE120101456). The authors acknowledge the use of equipment, scientific and technical assistance of the Curtin University Electron Microscope Facility, which is partially funded by the University, State and Commonwealth Governments of Australia, and the use of the instruments of the Scanning Probe Microscopy facility of the NRI/Department of Chemistry at Curtin University, funded by ARC LIEF grant number LE130100121. The authors also thank Dr. Leigh Aldous, Prof. Damien Arrigan for useful discussions and Dr. Junqiao Lee for performing the AFM characterisation.

References

(1) Timmer, B.; Olyhuis, W.; van den Berg, A. *Sens. Act. B* **2005**, *107*, 666-677.
(2) Liu, X.; Cheng, S.; Liu, H.; Hu, S.; Zhang, D.; Ning, H. *Sensors* **2012**, *12*, 9635-9665.
(3) Bakker, E. *Anal. Chem.* **2004**, *76*, 3285-3298.
(4) Opekar, F.; Stulik, K.: Electrochemical Gas Sensors. In *Encyclopedia of Analytical Chemistry*; John Wiley & Sons, Ltd.: Online, 2009; pp 1-24.
(5) Xiong, L.; Compton, R. G. *Int. J. Electrochem. Sci.* **2014**, *9*, 7152-7181.
(6) Buzzeo, M. C.; Hardacre, C.; Compton, R. G. *Anal. Chem.* **2004**, *76*, 4583-4588.
(7) Huang, X.-J.; Aldous, L.; O'Mahony, A. M.; del Campo, F. J.; Compton, R. G. *Anal. Chem.* **2010**, *82*, 5238-5245.
(8) Xiong, S.-Q.; Wei, Y.; Guo, Z.; Chen, X.; Wang, J.; Liu, J.-H.; Huang, X.-J. *J. Phys. Chem. C* **2011**, *115*, 17471-17478.
(9) Gębicki, J.; Kloskowski, A.; Chrzanowski, W.; Stepnowski, P.; Namiesnik, J. *Crit. Rev. Anal. Chem.* **2016**, *46*, 122-138.
(10) Rehman, A.; Zeng, X. *RSC Adv.* **2015**, *5*, 58371-58392.
(11) Silvester, D. S. *Analyst* **2011**, *136*, 4871-4882.
(12) Silvester, D. S.; Aldous, L.: Chapter 10: Electrochemical detection using ionic liquids. In *Electrochemical Strategies in Detection Science*; Arrigan, D. W. M., Ed.; RSC: Cambridge, UK, 2016.
(13) Barrosse-Antle, L. E.; Bond, A. M.; Compton, R. G.; O'Mahony, A. M.; Rogers, E. I.; Silvester, D. S. *Chem. Asian J.* **2010**, *5*, 202-230.
(14) Buzzeo, M. C.; Giovanelli, D.; Lawrence, N. S.; Hardacre, C.; Seddon, K. R.; Compton, R. G. *Electroanalysis* **2004**, *16*, 888-896.
(15) Ji, X.; Silvester, D. S.; Aldous, L.; Hardacre, C.; Compton, R. G. *J. Phys. Chem. C* **2007**, *111* 9562–9572.
(16) Murugappan, K.; Lee, J.; Silvester, D. S. *Electrochem. Commun.* **2011**, *13*, 1435-1438.
(17) Carter, M. T.; Stetter, J. R.; Findlay, M. W.; Patel, V. *ECS Trans.* **2012**, *50*, 211-220.
(18) Carter, M. T.; Stetter, J. R.; Findlay, M. W.; Patel, V. *ECS Trans.* **2014**, *64*, 95-103.
(19) Oudenhoven, J. F. M.; Knoben, W.; van Schaijk, R. *Procedia Eng.* **2015**, *120*, 983-986.
(20) Lee, J.; Silvester, D. S. *Analyst* **2016**, *141*, 3705–3713.
(21) Wang, J. *Electroanalysis* **2007**, *19*, 415-423.
(22) Heller, A.; Feldman, B. *Chem. Rev.* **2008**, *108*, 2482–2505.
(23) Pang, X.; Shaw, M. D.; Lewis, A. C.; Carpenter, L. J.; Batchellier, T. *Sens. Act. B* **2017**, *240*, 829-837.
(24) Malzahn, K.; Windmiller, J. R.; Valdes-Ramirez, G.; Schoning, M. l. J.; Wang, J. *Analyst* **2011**, *136*, 2912-2917.
(25) Lee, J.; Murugappan, K.; Arrigan, D. W. M.; Silvester, D. S. *Electrochim. Acta* **2013**, *101*, 158-168.
(26) Silvester, D. S.; Aldous, L.; Hardacre, C.; Compton, R. G. *J. Phys. Chem. B* **2007**, *111*, 5000-5007.
(27) Silvester, D. S.; Wain, A. J.; Aldous, L.; Hardacre, C.; Compton, R. G. *J. Electroanal. Chem.* **2006**, *596*, 131-140.
(28) Lee, J.; Arrigan, D. W. M.; Silvester, D. S. *Anal. Chem.* **2016**, *88*, 5104-5111.
(29) Burk, J. J.; Buratto, S. K. *J. Phys. Chem. C* **2013**, *117*, 18957−18966.
(30) Domínguez-Domínguez, S.; Arias-Pardilla, J.; Berenguer-Murcia, A.; Morallón, E.; Cazorla-Amorós, D. *J. Appl. Electrochem.* **2008**, *38*, 259-268.
(31) Kim, S.; Kwon, Y.; Jung, Y.; Park, S.-J. *Solid State Phenomena* **2007**, *124-124*, 1039-1042.
(32) Yasin, H. M.; Denuault, G.; Pletcher, D. *J. Electroanal. Chem.* **2009**, *633*, 327-332.
(33) Lee, J.; Du Plessis, G.; Arrigan, D. W. M.; Silvester, D. S. *Anal. Methods* **2015**, *7*, 7327-7335.
(34) Liu, Y.; Sairi, M.; Neusser, G.; Kranz, C.; Arrigan, D. W. M. *Anal. Chem.* **2015**, *87*, 5486−5490.
(35) Sairi, M.; Strutwolf, J.; Mitchell, R. A.; Silvester, D. S.; Arrigan, D. W. M. *Electrochim. Acta* **2013**, *101*, 177-185.
(36) Compton, R. G.; Banks, C. E.: *Understanding Voltammetry*; World Scientific: Singapore, 2007.
(37) Arrigan, D. W. M. *Analyst* **2004**, *129*, 1157-1165.
(38) Bond, A. M.; Luscombe, D.; Oldham, K. B.; Zoski, C. G. *J. Electroanal. Chem. Interfacial Electrochem.* **1988**, *249*, 1-14.
(39) Shoup, D.; Szabo, A. *J. Electroanal. Chem. Interfacial Electrochem.* **1982**, *140*, 237-245.
(40) Wang, X.; Li, G.; Liu, R.; Ding, H.; Zhang, T. *J. Mater. Chem.* **2012**, *22*, 21824-21827.